Commun. Math. Res.
doi: 10.4208/cmr.2025-0051

Vol. **x**, No. x, pp. 1-25
x 2026

A Positivity-Preserving Fourier Spectral Moving Mesh Method for the Keller-Segel Chemotaxis Model

Yutong Kuang[1] and Zhiwen Zhang[1,2,*]

[1] *Department of Mathematics, The University of Hong Kong, Hong Kong SAR 999077, P.R. China.*
[2] *Materials Innovation Institute for Life Sciences and Energy (MILES), HKU-SIRI, Shenzhen 518045, P.R. China.*

Received 27 November 2025; Accepted 4 January 2026

Abstract. We develop a numerical method for the Keller-Segel chemotaxis system that is designed to

(i) preserve the model's fundamental structural properties (positivity/bound preservation, mass conservation, and energy dissipation),

(ii) efficiently and accurately resolve the near-singular dynamics associated with spike formation and finite-time blow-up.

Our approach combines a linear, positivity-preserving scalar auxiliary variable (SAV) scheme (following the framework in [15]) with a Fourier spectral spatial discretization and an moving-mesh PDE-based method. The SAV reformulation provides a convenient platform for stable, linear time stepping while maintaining energy dissipation; the Fourier spectral discretization delivers high accuracy in smooth regions; and the moving-mesh PDE mesh redistribution concentrates collocation points in regions of large gradients so that sharp, localized structures can be resolved without prohibitive cost. We show that the proposed moving mesh SAV scheme inherits positivity preservation, mass conservation, and discrete energy dissipation provided the mesh motion avoids element overlap. Two-dimensional tests demonstrate the method's ability to capture fine spike profiles and estimate blow-up times with substantially reduced computational effort; the formulation extends straightforwardly to

*Corresponding author. *Email addresses:* yutongkuang@connect.hku.hk (Y. Kuang), zhangzw@hku.hk (Z. Zhang)

three spatial dimensions. Numerical results show that the proposed method is a practical and effective method for accurate simulation of chemotactic aggregation.

AMS subject classifications: 35K57, 65M50, 65M70, 92C17

Key words: Keller-Segel chemotaxis model, moving mesh PDE, scalar auxiliary variable, positivity preserving, finite-time blowup.

1 Introduction

Chemotaxis describes the directed movement and aggregation of organisms (such as microorganisms or cells) in response to chemical signals (commonly called chemoattractants). The classical Keller-Segel model (see Eqs. (2.1) and (2.2) in Section 2), proposed by Keller and Segel [19–21], uses the cell density $u(x,t)$ and the chemical concentration $\phi(x,t)$ as primary variables and models the competition between diffusion (Brownian motion) and aggregation driven by chemical gradients via advection-diffusion equations. As a result, the Keller-Segel system has become a fundamental mathematical model for studying biological aggregation, pattern formation, and processes such as tumor growth. The most common Keller-Segel system is written as a parabolic-parabolic system, i.e., for each organism and the chemical concentration, the evolution is described by a parabolic equation. In many cases, the chemical signals respond to the concentration of the organism much faster than the organism responds to the chemical signal. Therefore, it is common to simplify the parabolic equation for the chemical signal as an elliptic equation, which leads to a parabolic-elliptic system.

From a theoretical viewpoint, the Keller-Segel system has been intensively studied and has generated a rich body of results. In two spatial dimensions, it is well known that, for sufficiently large initial total mass, the parabolic-elliptic case [28] and certain fully parabolic cases [14] can develop finite-time aggregation (blow-up), where the solution concentrates toward Dirac-delta–type measures. Besides the classical δ-type singularity, self-similar profiles of the form $C(T-t+|x|^2)^{-1}$ have been identified and provide alternative descriptions of blow-up behavior in the 3D parabolic-elliptic case [13,30]. In three dimensions, global well-posedness results for the fully parabolic Keller-Segel system have been established under smallness assumptions on the initial data [3,22,27,32]. At the same time, a complete characterization (criteria and profile) of finite-time singularity formation in 3D for the fully parabolic case remains largely open.

Numerical simulations of the Keller-Segel model confront two distinct challenges. The first is to design discretizations that respect the model's fundamental

structural properties, i.e., positivity, mass conservation, and energy dissipation. The second is to reliably resolve the strong local gradients and potential finite-time concentration (blow-up) behaviors that the solutions may develop. A large body of work focuses on building discretizations that enforce one or more of the Keller-Segel model's structural properties. Some numerical schemes have been developed with positivity preserving conditions [1, 4, 6, 9, 10, 25, 34]. These schemes depend on particular spatial discretization, and some of them impose strict CFL restrictions on the time step. Recently, some unconditionally energy stable and positivity/bound preserving schemes have been proposed based on both nonlinear [5,29] and linear schemes [15]. However, these schemes encounter difficulties when simulating blow-up behaviors due to the lack of high resolution.

As mentioned above, solutions of the Keller-Segel model may develop large local variations or nearly singular spike profiles within small regions of the computational domain; using a uniform mesh to resolve such features is often prohibitively expensive. For this reason, moving mesh methods [17, 18, 23] that concentrate grid points in regions of steep gradients have become a standard practical strategy and have already been applied successfully to solve this kind of problem [7, 8, 24, 26, 33]. Moving-mesh PDE (MMPDE) approaches, and mesh redistribution techniques have also been successfully applied to chemotaxis problems: Budd *et al.* [2] employed an MMPDE-based moving mesh finite difference method to solve chemotactic systems in 1D; Sulman *et al.* [31] developed a positivity preserving moving mesh finite element method for 2D chemotactic systems based on the parabolic Monge-Ampère (PMA) method. Both works demonstrated that moving mesh methods provide good estimates of blow-up times and capture spike profiles efficiently.

Based on those existing algorithms, we aim to design an algorithm that is both accurate and computationally efficient for resolving the near-singular dynamics exhibited by Keller-Segel solutions while preserving the structural properties of the model. Spatial spectral discretization is a natural route to high accuracy at relatively low cost, while the adaptive mesh method is useful for computing singular behavior. To achieve our goals, we combine spectral spatial discretization with moving mesh strategies. A Fourier spectral implementation of MMPDE-based moving mesh methods has been developed by Feng *et al.* [11,12] and shown to work well for phase-field related equations. However, a direct implementation of a semi-implicit Fourier spectral method for the Keller-Segel system can easily break down the positivity. Fortunately, the unconditionally energy stable and bound-preserving linear schemes [15], based on the combination of function transform and the scalar auxiliary variable method, provide an ideal platform for the implementation of the Fourier spectral method. Building on the bound-

preserving SAV schemes, we develop an efficient and accurate numerical method by combining the MMPDE-based moving mesh method in two dimensions. The approach is straightforward to extend to three spatial dimensions. The bound-preserving, mass conservation, and energy dissipation properties are inherited if the mesh does not overlap during the moving process. Numerical results show that our algorithm can resolve the fine structures and capture near blow-up patterns efficiently.

The paper is organized as follows. In Section 2, we briefly introduce the classic Keller-Segel system and its blow-up behavior, and then we construct a first-order positivity preserving SAV scheme based on the work in [15]. Section 3 introduces the MMPDE-based Fourier spectral moving mesh method and outlines our proposed moving mesh positivity preserving SAV scheme for solving the fully parabolic Keller-Segel system. In Section 4, we present numerical results to demonstrate the performance of our method. Concluding remarks are given in Section 5.

2 Preliminaries

In this section, we provide some basic background on Keller-Segel models and introduce the positivity-preserving and energy stable scheme based on the SAV approach and the function transform approach.

2.1 Keller-Segel system and blow up behaviors

We consider the following Keller-Segel system with a single organism and a single chemoattractant in a bounded domain Ω:

$$\frac{\partial u}{\partial t} = D\big(\gamma\Delta u - \chi\nabla\cdot(\eta(u)\nabla\phi)\big), \tag{2.1}$$

$$\tau\frac{\partial \phi}{\partial t} = \mu\Delta\phi - \alpha\phi + \chi u \tag{2.2}$$

with periodic boundary conditions.

Here, the unknowns are u, the concentration of the organism, and ϕ, the concentration of the chemoattractant. The Eq. (2.1) of u models the evolution of the density of the organism. The organism diffuses with mobility γ and drifts in the direction of $\nabla\phi$ with velocity $\chi\nabla\phi$. The function $\eta(u)$ describes the concentration-dependent mobility, and different choices of $\eta(u)$ correspond to different models. Note that in this work, we mainly focus on the classic case ($\eta(u)=u$). The Eq. (2.2) of ϕ models the evolution of the concentration of chemoattractant, whose production rate is proportional to u.

The parameters D,γ,χ,τ,μ and α are all positive. Among them, χ and τ play particularly important roles: χ represents the chemotactic sensitivity, and τ characterizes how fast the chemoattractant concentration ϕ responds to the organism concentration u. When $\tau>0$, the system is referred to as the parabolic-parabolic Keller-Segel system, while for $\tau=0$ it reduces to the parabolic-elliptic case, which assumes that the chemoattractant released by the organisms reaches equilibrium instantaneously.

The Eqs. (2.1) and (2.2), together with periodic boundary conditions, can be interpreted as a gradient flow with respect to (u,ϕ). For this case, we set $f(u)=u\ln u-u$ such that

$$f''(u)=\frac{1}{\eta(u)}=\frac{1}{u},$$

and define the following free energy:

$$E[u,\phi]=\int_\Omega\left(\gamma f(u)-\chi u\phi+\frac{\mu}{2}|\nabla\phi|^2+\frac{\alpha}{2}\phi^2\right)dx. \tag{2.3}$$

By noting that

$$\Delta u=\nabla\cdot\left(\frac{1}{f''(u)}\nabla f'(u)\right)=\nabla\cdot(u\nabla\ln u),$$

we can rewrite Eqs. (2.1) and (2.2) as

$$\frac{\partial u}{\partial t}=D\nabla\cdot\left(\frac{1}{f''(u)}\nabla(\gamma\ln u-\chi\phi)\right)=D\nabla\cdot\left(u\nabla\frac{\delta E}{\delta u}\right), \tag{2.4}$$

$$\tau\frac{\partial\phi}{\partial t}=\mu\Delta\phi-\alpha\phi+\chi u=-\frac{\delta E}{\delta\phi}. \tag{2.5}$$

Taking the inner products of (2.4) with $\delta E/\delta u$, and of (2.5) with $\partial\phi/\partial t$, and summing up the results, we obtain the energy dissipation law

$$\frac{dE[u(t),\phi(t)]}{dt}=-\int_\Omega\left[Du\left(\nabla\frac{\delta E}{\delta u}\right)^2+\tau\left(\frac{\partial\phi}{\partial t}\right)^2\right]dx, \tag{2.6}$$

where $\delta E/\delta u=\gamma\ln u-\chi\phi$. In the classical case, the concentration-dependent mobility $\eta(u)=u$. Therefore, we must ensure $u\geq 0$ for the energy dissipation law to hold, which requires numerical algorithms to preserve positivity. In addition, the Keller-Segel system with periodic boundary conditions also satisfies the mass conservation property

$$\frac{d}{dt}\int_\Omega u dx=0. \tag{2.7}$$

For this classical system ($\eta(u)=u$), extensive mathematical analyses of blow-up behavior have been conducted. In particular, in the two-dimensional case, whether blow up occurs depends on the total mass of u, i.e., $m=\int_\Omega u dx$. The well-known Keller-Segel dichotomy (critical collapse) states that 8π is the critical mass for the simplest two-dimensional parabolic-elliptic Keller-Segel system in $\Omega=\mathbb{R}^2$, namely Eqs. (2.1) and (2.2) with $D=\chi=\gamma=\mu=1$ and $\tau=\alpha=0$, i.e.

$$\begin{aligned} &u_t=\nabla\cdot(\nabla u-u\nabla\phi),\\ &\Delta\phi=-u. \end{aligned} \tag{2.8}$$

The above system exhibits a critical behavior: the solution either remains global and bounded or blows up in finite time, depending on the initial total mass of the density u. Specifically, we have

1. If $m_0<8\pi$, the system has a global smooth solution.

2. If $m_0>8\pi$, the system blows up in finite time in the sense of the $|\cdot|_\infty$ norm.

It can be seen from the classical variance identity for system (2.8) [28], that,

$$\frac{d}{dt}\int_{x\in\mathbb{R}^2}|x|^2u(x)dx=\frac{m_0}{2\pi}(8\pi-m_0). \tag{2.9}$$

Then, the solution of (2.8) exhibits a quantized concentration of mass at the origin, which is a type of blow up known as δ-blow up. In higher dimensions, the evolution of the Keller-Segel system becomes more complicated. Nevertheless, the coexistence of blow-up and global smooth solutions still depends on the size of the initial data, though we do not summarize those results here.

2.2 Positivity preserving SAV scheme

Now we introduce a numerical scheme that is linear, positivity preserving, and unconditionally energy stable for any consistent spatial discretization. The core idea in this approach is to combine the SAV approach with the function transform approach:

(1) the positivity preserving property is enforced by making a suitable function transform,

(2) the linearity and unconditionally energy stability are achieved through the SAV formulation.

Due to the form of $f(u)$, the range of numerical solution must remain in $(0,+\infty)$. A common strategy to enforce solutions to preserve bounds or positivity is to apply a suitable function transform. Here, we consider the transform

$$u=\exp(v). \tag{2.10}$$

The above transform guarantees that the numerical solution of u stays in $(0,+\infty)$. Since ϕ does not need to be bound preserving, we do not transform ϕ.

Substituting the term (2.10) into Eq. (2.1), we obtain the equation for v

$$\frac{\partial v}{\partial t}=D\left[\gamma(\Delta v+|\nabla v|^2)-\chi(\Delta\phi+\nabla v\cdot\nabla\phi)\right]. \tag{2.11}$$

To obtain a linear and energy dissipative scheme for the transformed system, the SAV approach is considered. We first split the free energy $E[u,\phi]$ into two parts as follows:

$$\begin{aligned}E[u,\phi]&=\int_\Omega\left(\gamma f(u)-\chi u\phi+\frac{\alpha}{4}\phi^2\right)dx+\int_\Omega\left(\frac{\mu}{2}|\nabla\phi|^2+\frac{\alpha}{4}\phi^2\right)dx\\&=E_1[u,\phi]+E_0[\phi].\end{aligned} \tag{2.12}$$

In the case that the system has a global smooth solution, it is easy to see that there exists $C_0>0$ such that

$$E_1[u,\phi]\geq -C_0+1, \tag{2.13}$$

because u is bounded in this case and f is strictly convex when $u>0$. While in the blow-up case, u is not bounded, and thus we cannot theoretically prove (2.13). However, in the numerical simulation, we can assume u is bounded and choose a large enough C_0. Therefore, we can assume that there exists $C_0>0$ satisfying condition (2.13) in the numerical implementation.

As in the SAV approach, we introduce a SAV to enforce energy dissipation (2.6). More precisely, we introduce $r(t)=E_1(u,\phi)+C_0\geq 1$. Then, we have

$$E[u,\phi]=\frac{\mu}{2}(\phi,-\Delta\phi)_\Omega+\frac{\alpha}{4}(\phi,\phi)_\Omega+r=E_0(\phi)+r, \tag{2.14}$$

$$\frac{d}{dt}E[u,\phi]=\mu(\phi_t,-\Delta\phi)_\Omega+\frac{\alpha}{2}(\phi_t,\phi)_\Omega+r_t=\frac{dE_0(\phi)}{dt}+r_t. \tag{2.15}$$

By combining the positivity preserving transform and the energy dissipation SAV scheme, we can reformulate (2.1), (2.2), and (2.6) to

$$\frac{\partial v}{\partial t}=D\left[\gamma(\Delta v+|\nabla v|^2)-\chi(\Delta\phi+\nabla v\cdot\nabla\phi)\right], \tag{2.16}$$

$$u=\exp(v), \tag{2.17}$$

$$\tau\frac{\partial\phi}{\partial t}=\mu\Delta\phi-\alpha\phi+\chi u, \tag{2.18}$$

$$\frac{dE_0(\phi)}{dt}+r_t=-\frac{E_0(\phi)+r(t)}{E(u,\phi)+C_0}\int_\Omega\left[Du\left(\nabla\frac{\delta E}{\delta u}\right)^2+\tau\left(\frac{\partial\phi}{\partial t}\right)^2\right]dx. \tag{2.19}$$

Using the semi-implicit time discretization, we now construct a first-order scheme for the above system in a uniform setting, and higher order ($k\leq 6$) schemes can also be constructed similarly based on the BDF-Adams-Bashforth SAV techniques [15]. Given (v^n,u^n,ϕ^n,r^n), we compute $(v^{n+1},u^{n+1},\phi^{n+1},r^{n+1})$ as follows:

$$\frac{v^{n+1}-v^n}{\delta t}=D\gamma\Delta v^{n+1}+D\gamma|\nabla v^n|^2-D\chi(\Delta\phi^n+\nabla v^n\cdot\nabla\phi^n), \tag{2.20}$$

$$\bar{u}^{n+1}=\exp(v^{n+1}), \tag{2.21}$$

$$\lambda^{n+1}\int_\Omega\bar{u}^{n+1}dx-\int_\Omega u^n dx=0, \tag{2.22}$$

$$u^{n+1}=\lambda^{n+1}\bar{u}^{n+1}, \tag{2.23}$$

$$\tau\frac{\bar{\phi}^{n+1}-\bar{\phi}^n}{\delta t}=\mu\Delta\bar{\phi}^{n+1}-\alpha\bar{\phi}^{n+1}+\chi u^{n+1}, \tag{2.24}$$

$$\begin{aligned}&\frac{1}{\delta t}\left(E_0(\bar{\phi}^{n+1})-E_0(\bar{\phi}^n)+r^{n+1}-r^n\right)\\&=-\frac{E_0(\bar{\phi}^{n+1})+r^{n+1}}{E[\bar{u}^{n+1},\bar{\phi}^{n+1}]+C_0}\int_\Omega\left[D\bar{u}^{n+1}\left(\nabla\frac{\delta E}{\delta u}(\bar{u}^{n+1})\right)^2+\tau\left(\frac{\bar{\phi}^{n+1}-\bar{\phi}^n}{\delta t}\right)^2\right]dx,\end{aligned} \tag{2.25}$$

$$\eta^{n+1}=\frac{E_0(\bar{\phi}^{n+1})+r^{n+1}}{E[\bar{u}^{n+1},\bar{\phi}^{n+1}]+C_0}, \tag{2.26}$$

$$\phi^{n+1}=\eta_k^{n+1}\bar{\phi}^{n+1}. \tag{2.27}$$

Note that in the above numerical scheme, (2.20) and (2.24) are first-order semi-implicit schemes for (2.16) and (2.18), while (2.22) is first-order approximation to the mass conservation condition (2.7). We summarize that v^{n+1}, λ^{n+1}, u^{n+1}, $\bar{\phi}^{n+1}$ are first-order approximations of $v(t_{n+1})$, 1, $u(t_{n+1})$, $\phi(t_{n+1})$. Eq. (2.25) is also a first-order approximation to (2.19), which implies that r^{n+1} is a first-order approximation to $r(t_{n+1})$. Then, with the fact that (2.26) implies $\eta^{n+1}=1+\mathcal{O}(\delta t)$, we deduce that ϕ^{n+1} is a first-order approximation to $\phi(t_{n+1})$.

The above scheme has the following unconditional properties (see Shen *et al.* [15]):

Theorem 2.1. *Given u^n, ϕ^n, v^n and r^n such that*

$$\int_\Omega u^n dx = \int_\Omega u^0 dx. \tag{2.28}$$

Then, the scheme (2.20)-(2.27) *admits a unique solution satisfying the following properties unconditionally:*

1. *Positivity preserving: $u^{n+1} > 0$.*
2. *Mass conservation: $\int_\Omega u^{n+1} dx = \int_\Omega u^0 dx$.*
3. *Energy dissipation with a modified energy defined by $\bar{E}^n = E_0(\bar{\phi}^n) + r^n$. More precisely, if $\bar{E}^n \geq 0$, we have $\bar{E}^{n+1} \geq 0, \eta^{n+1} \geq 0$ and*

$$\begin{aligned} &\bar{E}^{n+1} - \bar{E}^n \\ &= -\eta^{n+1} \int_\Omega \left[D\bar{u}^{n+1} \left(\nabla \frac{\delta E}{\delta u}(\bar{u}^{n+1}) \right)^2 + \tau \left(\frac{\bar{\phi}^{n+1} - \bar{\phi}^n}{\delta t} \right)^2 \right] dx \leq 0. \end{aligned} \tag{2.29}$$

4. *There exists constant M such that*

$$\sqrt{E_0(\phi^n)} = \sqrt{\int_\Omega \left(\frac{\mu}{2} |\nabla \phi^n|^2 + \frac{\alpha}{4} (\phi^n)^2 \right) dx} \leq M, \quad \forall n. \tag{2.30}$$

3 A Fourier spectral moving mesh method for Keller-Segel equations

In this section, we will present our scheme that combines the Fourier spectral moving mesh method and the positivity preserving SAV scheme for efficiently and accurately solving the Keller-Segel models, especially for the blow-up cases. We first introduce the MMPDEs and their Fourier spectral implementation, and then we present our numerical scheme.

3.1 Formulation and Fourier spectral implementation of moving mesh PDEs

To efficiently capture blow-up behaviors, it is essential to use an adaptive procedure in which mesh points cluster close to the regions where singularities develop. There are various approaches to achieve this goal, including *h*-refinement,

where mesh points are successively added in the singular region, and r-refinement, where a fixed number of mesh points move according to the singularity or large gradients. For successful integration with the spectral method, we consider an r-refinement method in which the mesh points evolve according to an MMPDE. MMPDEs can be formulated either on the physical domain or on the computational domain. In this paper, as in [11, 12], we consider the former one, which is derived more rigorously though slightly more complicated. In this approach, the criteria for redistributing the mesh are expressed through certain variational principles. There are also other adaptive strategies, such as the parabolic Monge-Ampère method [31].

To be more specific, the moving mesh method redistributed a fixed number of grid nodes continuously in time to obtain higher grid density in regions of large solution variation in the physical domain Ω_p (parameterized by x). This is achieved by smoothing the gradient in the computational domain Ω_c (parameterized by ξ) with uniformly distributed grids. Therefore, a mapping $x=x(\xi,t)$: $\Omega_c \to \Omega_p$ is constructed from the computational domain to the physical domain such that the transformed solution $v(\xi)=u(x(\xi))$ behaves more regularly in the computational domain [11].

For the physical domain-based variational formulation (PDVF) [16] considered here, we consider finding the inverse map $\xi(x,t)$ of $x(\xi,t)$. Given an approximate monitor function ω that links the mesh with the physical solution u, the mapping is obtained by solving the following variational problem in one dimension:

$$\min_{\xi(x,t)} I[\xi]=\int_{\Omega_p} \omega^{-1}\left(\frac{\partial \xi}{\partial x}\right)^2 \mathrm{d}x, \tag{3.1}$$

so that the mesh concentrates where ω is large. A particular form of ω, which is adopted in this paper, is given by

$$\omega=\left(1+\alpha|\nabla_{\xi} u|^2\right)^{\frac{1}{\gamma}}, \tag{3.2}$$

where $\alpha,\gamma>0$ are problem dependent parameters. In higher dimensions, the objective function in (3.1) becomes

$$I[\xi]=\int_{\Omega_p}\sum_i \left(\nabla_x \xi^i\right)^T G^{-1}\nabla_x \xi^i \,\mathrm{d}x, \tag{3.3}$$

where G is the matrix monitor function. In this paper, we adopt the Winslow type of monitor function $G=\omega I$. Other forms of G allow the introduction of anisotropically distributed mesh points.

The variational problem (3.3) can be solved numerically via its gradient flow, in other words, the moving mesh PDE

$$\frac{\partial}{\partial t}\xi^i(x,t) = p\nabla_x \cdot \left(G^{-1}\nabla_x \xi^i\right), \quad i=1,2,3, \tag{3.4}$$

where the mobility p is a positive function that may vary in space. By introducing the covariant and contravariant basis vectors as in [16]

$$a_i = \frac{\partial x}{\partial \xi^i}, \quad a^i = \nabla_x \xi^i, \quad i=1,2,3, \tag{3.5}$$

and the Jacobian $J = a_1 \cdot (a_2 \times a_3)$, the Eq. (3.4) can be transformed into a more convenient form in the computational domain

$$\frac{\partial x}{\partial t} = p\left[\sum_{i,j}\left(a^i \cdot G^{-1}a^j\right)\frac{\partial^2 x}{\partial \xi^i \partial \xi^j} - \sum_{i,j}\left(a^i \cdot \frac{\partial G^{-1}}{\partial \xi^j}a^j\right)\frac{\partial x}{\partial \xi^i}\right]. \tag{3.6}$$

For the Winslow type of monitor function $G = \omega I$ used here, the above equation can be further simplified to

$$\frac{\partial x}{\partial t} = \frac{p}{\omega^2}\sum_{i,j}\left(a^i \cdot a^j\right)\frac{\partial}{\partial \xi^i}\left(\omega\frac{\partial x}{\partial \xi^j}\right). \tag{3.7}$$

Here we adopt the variable mobility $p = \mu\omega^2/\lambda$ in practical computations, where λ is the largest eigenvalue of the positive-definite matrix $A = (A_{i,j}) = (a^i \cdot a^j)$ and the generic constant μ controls the artificial time scale of the MMPDE as compared with the physical time t. More discussions on the choice of mobility function p can be found in [16].

Next, we describe the Fourier spectral implementation of the above MMPDE. In [11], periodic boundary conditions are imposed on the MMPDE, thus allowing the implementation of the Fourier spectral method. This method has already been successfully applied to phase-field simulations such as the Allen-Cahn [11] and Cahn-Hilliard [12] equations.

To introduce this method, let the computational domain be the unit square $[0,1]\times[0,1]$. It is the displacement of the adaptive grid point from its inverse image on the regular grid, i.e., $x(\xi,t)-\xi$, that satisfies the periodic boundary conditions on the unit square, that is,

$$x\left(\xi+(k,l),t\right) = x(\xi,t)+(k,l), \quad \forall (k,l)\in\mathbb{Z}^2. \tag{3.8}$$

Note that this condition does not require that $x(\xi,t)$ maps the unit square onto itself, i.e., the physical domain may not turn out to be a square even though the computational domain is. Illustrations are shown in [11]. Although the physical domain boundaries are curved, the condition (3.8) implies that the periodic copies of Ω_p (non-square) cover the whole two-dimensional space as effectively as periodic copies of the unit square, which is harmonious with the periodic condition in the Keller-Segel equations.

For the MMPDE (3.7) here, with periodic conditions on $X = x-\xi$, its form becomes

$$\frac{\partial X}{\partial t} = \mu \sum_{i,j} \frac{a^i \cdot a^j}{\lambda} \frac{\partial}{\partial \xi^i} \left[\omega \left(\frac{\partial X}{\partial \xi^j} + e^j \right) \right], \tag{3.9}$$

where e^i denotes the canonical unit vector. Then the semi-implicit Fourier spectral method can be applied to solve this nonlinear equation numerically [11]. In the Fourier space, the discretized equation reads

$$\left(1+\mu W \Delta t k^2\right)\left(\widehat{\bar{X}} - \widehat{X}\right) = \mu \Delta t \left\{ \sum_{i,j} \frac{a^i \cdot a^j}{\lambda} \frac{\partial}{\partial \xi^i} \left[\omega \left(\frac{\partial X}{\partial \xi^j} + e^j \right) \right] \right\}^{\wedge}, \tag{3.10}$$

where $\bar{X}$ demotes the value of X at the next time step, k is the wave vector, W is the maximum of ω over Ω_c introduced by semi-implicit scheme, and $\wedge$ represents the Fourier transform.

3.2 A Fourier spectral moving mesh positivity preserving SAV scheme

We now consider the moving mesh transformation: $x = x(\xi,t): \Omega_c \to \Omega_p$, mapping the computational domain Ω_c (parameterized by ξ) to the physical domain Ω_p (parameterized by x). By applying this variable transformation $x = x(\xi,t)$ to the Keller-Segel equations and treating u and ϕ as functions of ξ and t, Eqs. (2.1) and (2.2) become the following system:

$$\frac{\partial}{\partial t} u(\xi,t) = \dot{x} \cdot \nabla_x u + D\left(\gamma \Delta_x u - \chi \nabla_x \cdot (u \nabla_x \phi)\right), \tag{3.11}$$

$$\tau \frac{\partial}{\partial t} \phi(\xi,t) = \tau \dot{x} \cdot \nabla_x \phi + \mu \Delta_x \phi - \alpha \phi + \chi u, \tag{3.12}$$

where the dot denotes the time derivative of the physical mesh position, $\dot{x} = \partial_t x(\xi,t)$. Under the transformation, the free energy (2.3) becomes

$$E[u,\phi] = \int_{\Omega_c} \left(\gamma f(u) - \chi u \phi + \frac{\mu}{2} |\nabla_x \phi|^2 + \frac{\alpha}{2} \phi^2 \right) J(\xi,t) d\xi, \tag{3.13}$$

where $J(\xi,t)=\partial x/\partial\xi$ is the Jacobian. Similarly, the energy dissipation law on the computational domain reads

$$\frac{dE[u(t),\phi(t)]}{dt}=-\int_{\Omega_c}\left[Du\left(\nabla_x\frac{\delta E}{\delta u}\right)^2+\tau\left(\frac{\partial\phi}{\partial t}-\dot{x}\cdot\nabla_x\phi\right)^2\right]J(\xi,t)d\xi, \tag{3.14}$$

and mass conservation becomes

$$\frac{d}{dt}\int_\Omega u(\xi,t)J(\xi,t)d\xi=0. \tag{3.15}$$

We note from Eq. (3.11) that the moving mesh method brings a mesh velocity term $\dot{x}\cdot\nabla_x u$ to the original equation. And the large gradient in the blow-up behavior is mainly caused by the advective term $\nabla_x u\cdot\nabla_x\phi$ in the nonlinear aggregative term $\nabla_x\cdot(u\nabla_x\phi)$. Therefore, the mesh velocity term can be seen as an advective correction term and reduces the relative aggregative transport seen on the computational mesh. This provides an intuitive explanation for why the moving mesh method improves the resolution of steep gradients in Keller-Segel simulations.

Because we focus on the two-dimensional case, we now give the 2D computational representation of $\nabla_x u$ and $\Delta_x u$ in the computational domain Ω_c for convenience. The contravariant basis vectors are

$$a^1=\nabla\xi^1=\frac{1}{J}\left(\frac{\partial x_2}{\partial\xi^2},-\frac{\partial x_1}{\partial\xi^2}\right),\quad a^2=\nabla\xi^2=\frac{1}{J}\left(-\frac{\partial x_2}{\partial\xi^1},\frac{\partial x_1}{\partial\xi^1}\right), \tag{3.16}$$

and the Jacobian is

$$J=\frac{\partial x_1}{\partial\xi^1}\frac{\partial x_2}{\partial\xi^2}-\frac{\partial x_1}{\partial\xi^2}\frac{\partial x_2}{\partial\xi^1}. \tag{3.17}$$

Then the physical gradient can be written as

$$\nabla_x u=\sum_i a^i\frac{\partial u}{\partial\xi^i}=\frac{1}{J}\left(\frac{\partial x_2}{\partial\xi^2}\frac{\partial u}{\partial\xi^1}-\frac{\partial x_2}{\partial\xi^1}\frac{\partial u}{\partial\xi^2},-\frac{\partial x_1}{\partial\xi^2}\frac{\partial u}{\partial\xi^1}+\frac{\partial x_1}{\partial\xi^1}\frac{\partial u}{\partial\xi^2}\right), \tag{3.18}$$

and the Laplacian becomes

$$\Delta_x u=\frac{1}{J}\nabla_\xi\cdot(JA\nabla_\xi u),\quad \big(A=(A_{i,j})=(a^i\cdot a^j),\ i,j=1,2\big), \tag{3.19}$$

where

$$A\nabla_\xi u=\begin{bmatrix} a_{11}\dfrac{\partial u}{\partial\xi_1}+a_{12}\dfrac{\partial u}{\partial\xi_2} \\ a_{21}\dfrac{\partial u}{\partial\xi_1}+a_{22}\dfrac{\partial u}{\partial\xi_2}\end{bmatrix}. \tag{3.20}$$

Although we do not present higher-dimensional simulations here, the method extends naturally to higher dimensions [11].

To obtain an efficient and energy stable time discretization on the computational domain to solve the Eqs. (3.11) and (3.12), we combine the positivity preserving SAV scheme mentioned in Section 2.2. Using the function transform $u=\exp(v)$ and the scalar auxiliary variable $r(t)$, the transformed system on Ω_c can be reformulated as

$$\frac{\partial}{\partial t}v(\xi,t)=\dot{x}\cdot\nabla_x v+D\left[\gamma(\Delta_x v+|\nabla_x v|^2)-\chi(\Delta_x\phi+\nabla_x v\cdot\nabla_x\phi)\right], \tag{3.21}$$

$$u=\exp(v), \tag{3.22}$$

$$\tau\frac{\partial}{\partial t}\phi(\xi,t)=\tau\dot{x}\cdot\nabla_x\phi+\mu\Delta_x\phi-\alpha\phi+\chi u, \tag{3.23}$$

$$\begin{aligned}&\frac{dE_0(\phi)}{dt}+r_t\\&=-\frac{E_0(\phi)+r(t)}{E(u,\phi)+C_0}\int_\Omega\left[Du\left(\nabla_x\frac{\delta E}{\delta u}\right)^2+\tau\left(\frac{\partial\phi}{\partial t}-\dot{x}\cdot\nabla_x\phi\right)^2\right]J(\xi,t)d\xi,\end{aligned} \tag{3.24}$$

where $E_0(\phi)$ and $r(t)\geq 1$ are defined by

$$E_0(\phi)=\int_{\Omega_c}\left(\frac{\mu}{2}|\nabla_x\phi|^2+\frac{\alpha}{4}\phi^2\right)J(\xi,t)d\xi, \tag{3.25}$$

$$r(t)=E_1(u,\phi)+C_0=\int_{\Omega_c}\left[\gamma(u\ln u-u)-\chi u\phi+\frac{\alpha}{4}\phi^2\right]J(\xi,t)d\xi+C_0. \tag{3.26}$$

We now deduce the first-order scheme for the above system on the computational domain Ω_c. To apply the semi-implicit Fourier spectral scheme, we denote by λ^* the maximum among the eigenvalues of A over Ω_c. Define the following term:

$$\begin{aligned}E_{diss}=\int_{\Omega_c}\Bigg[&D\bar{u}^{n+1}\left(\nabla_x\frac{\delta E}{\delta u}(\bar{u}^{n+1})\right)^2\\&+\tau\left(\frac{\bar{\phi}^{n+1}-\bar{\phi}^n}{\delta t}-\dot{x}\cdot\nabla_x\bar{\phi}^{n+1}\right)^2\Bigg]J(\xi,t)d\xi.\end{aligned} \tag{3.27}$$

Then, given (v^n,u^n,ϕ^n,r^n), we find $(v^{n+1},u^{n+1},\phi^{n+1},r^{n+1})$ as follows:

$$\begin{aligned}&\frac{v^{n+1}-v^n}{\delta t}-\lambda^*D\gamma\Delta_\xi v^{n+1}\\&=\dot{x}\cdot\nabla_x v^n+D\gamma\Delta_x v^n+D\gamma|\nabla_x v^n|^2\\&\quad-D\chi(\Delta_x\phi^n+\nabla_x v^n\cdot\nabla_x\phi^n)-\lambda^*D\gamma\Delta_\xi v^n,\end{aligned} \tag{3.28}$$

$$\bar{u}^{n+1}=\exp(v^{n+1}), \tag{3.29}$$

$$\lambda^{n+1}\int_{\Omega_c}\bar{u}^{n+1}J(\xi,t_{n+1})d\xi-\int_{\Omega_c}u^nJ(\xi,t_n)d\xi=0, \tag{3.30}$$

$$u^{n+1}=\lambda^{n+1}\bar{u}^{n+1}, \tag{3.31}$$

$$\begin{aligned}&\tau\frac{\bar{\phi}^{n+1}-\bar{\phi}^n}{\delta t}-\mu\lambda^*\Delta_\xi\bar{\phi}^{n+1}\\&=\tau\dot{x}\cdot\nabla_x\bar{\phi}^n+\mu\Delta_x\bar{\phi}^n-\alpha\bar{\phi}^{n+1}+\chi u^{n+1}-\mu\lambda^*\Delta_\xi\bar{\phi}^n,\end{aligned} \tag{3.32}$$

$$\begin{aligned}&\frac{1}{\delta t}\Big(E_0(\bar{\phi}^{n+1})-E_0(\bar{\phi}^n)+r^{n+1}-r^n\Big)\\&=-\frac{E_0(\bar{\phi}^{n+1})+r^{n+1}}{E[\bar{u}^{n+1},\bar{\phi}^{n+1}]+C_0}E_{diss}\big(\bar{u}^{n+1},\bar{\phi}^{n+1},\bar{\phi}^n,\dot{x}\big),\end{aligned} \tag{3.33}$$

$$\eta^{n+1}=\frac{E_0(\bar{\phi}^{n+1})+r^{n+1}}{E[\bar{u}^{n+1},\bar{\phi}^{n+1}]+C_0}, \tag{3.34}$$

$$\phi^{n+1}=\eta^{n+1}\bar{\phi}^{n+1}. \tag{3.35}$$

Here, the term $\tau((\bar{\phi}^{n+1}-\bar{\phi}^n)/\delta t-\dot{x}\cdot\nabla_x\bar{\phi}^{n+1})^2$ that appears in (3.27) may be computed as

$$\frac{(\mu\Delta_x\bar{\phi}^{n+1}-\alpha\bar{\phi}^{n+1}+\chi u^{n+1})^2}{\tau} \tag{3.36}$$

in practical computation using the Eq. (3.12), since in this way we can avoid evaluating the Jacobian in two separate time levels. The counterpart of (3.28) and (3.32) in the Fourier space conjugate to Ω_c reads

$$\begin{aligned}&\big(1+\lambda^*\delta tD\gamma k^2\big)\big(\widehat{v}^{n+1}-\widehat{v}^n\big)\\&=\delta t\Big\{\dot{x}\cdot\nabla_xv^n+D\gamma\Delta_xv^n+D\gamma|\nabla_xv^n|^2-D\chi(\Delta_x\phi^n+\nabla_xv^n\cdot\nabla_x\phi^n)\Big\}^\wedge,\end{aligned} \tag{3.37}$$

$$\begin{aligned}&\big[\tau+\delta t(\alpha+\mu\lambda^*k^2)\big]\widehat{\bar{\phi}}^{n+1}\\&=\delta t\big(\mu\Delta_x\bar{\phi}^n+\tau\dot{x}\cdot\nabla_x\bar{\phi}^n\big)^\wedge+\delta t\chi\widehat{u}^{n+1}+\big(\tau+\delta t\mu\lambda^*k^2\big)\widehat{\bar{\phi}}^n.\end{aligned} \tag{3.38}$$

Note that in the monitor function $\omega=(1+\alpha|\nabla_\xi v|^2)^{1/\gamma}$ we need to compute $\nabla_\xi v$. However, the blow-up point where we want mesh points to concentrate is a maximum of the solution. If we compute $\nabla_\xi v$ using FFT-based differentiation, the gradient at that maximum will be zero. Indeed, not only the blow-up point, but all the directional derivatives of those maximal points in this direction will be zero. Therefore, when simulating blow-up solutions, we need to implement a first-order finite difference approximation to compute the directional derivatives on those maximal points. This treatment differs from the phase-field simulations in [11,12].

Then the efficient implementation of the above scheme with moving mesh PDE can be summarized as Algorithm 1.

Algorithm 1: Moving-mesh SAV Scheme Implementation

Input: u^n, ϕ^n, r^n, x^n, timestep δt.
Output: $u^{n+1}, \phi^{n+1}, r^{n+1}, x^{n+1}$.
for $n=0,1,2,\ldots$ **do**

1. Determine physical mesh x^{n+1} from MMPDE (3.9) and compute mesh velocity $\dot{x}$.
2. Solve v^{n+1} from (3.28).
3. Compute $\bar{u}^{n+1}$ from (3.29) and compute λ^{n+1} explicitly from (3.30).
4. Update u^{n+1} from (3.31).
5. With u^{n+1} known, solve $\bar{\phi}^{n+1}$ from (3.32).
6. With $\bar{u}^{n+1}, \bar{\phi}^{n+1}$ known, determine r^{n+1} explicitly from (3.33).
7. Compute η^{n+1} from (3.34) and update ϕ^{n+1} from (3.35).

The above scheme is based on a first-order positivity preserving SAV scheme, and it successfully inherits the energy stable quality from the original scheme as long as the moving mesh method is good enough. We have the following results:

Theorem 3.1. *Assume the Jacobian $J(\xi,t)>0$ and $E_1(u,\phi)+C_0\geq 1$. Given $u^n>0, \phi^n, v^n$ and r^n such that*

$$\int_{\Omega_c} u^n J(\xi,t_n)d\xi = \int_{\Omega_c} u^0 J(\xi,t_0)d\xi. \tag{3.39}$$

Then, the scheme (3.28)-(3.35) *admits a unique solution satisfying the following properties:*

1. *Positivity preserving: $u^{n+1}>0$.*
2. *Mass conservation: $\int_{\Omega_c} u^{n+1} J(\xi,t_{n+1})d\xi = \int_{\Omega_c} u^0 J(\xi,t_0)d\xi$.*
3. *Energy dissipation with a modified energy defined by $\bar{E}^n = E_0(\bar{\phi}^n)+r^n$. More precisely, if $\bar{E}^n\geq 0$, we have $\bar{E}^{n+1}\geq 0, \eta^{n+1}\geq 0$ and*

$$\bar{E}^{n+1}-\bar{E}^n = -\eta^{n+1}\delta t E_{diss}\left(\bar{u}^{n+1},\bar{\phi}^{n+1},\bar{\phi}^n,\dot{x}\right)\leq 0. \tag{3.40}$$

4. There exists constant M such that

$$\sqrt{E_0(\phi^n)}=\sqrt{\int_{\Omega_c}\Big(\frac{\mu}{2}|\nabla\phi^n|^2+\frac{\alpha}{4}(\phi^n)^2\Big)J(\xi,t_n)d\xi}\le M,\quad \forall n. \tag{3.41}$$

Proof. We can derive from (3.29) that $\bar{u}^{n+1}\ge 0$. Then, from (3.30), we deduce that

$$\lambda^{n+1}\int_{\Omega_c}\bar{u}^{n+1}J(\xi,t_{n+1})d\xi=\int_{\Omega_c}u^0J(\xi,t_0)d\xi,$$

which implies $\lambda^{n+1}>0$, and consequently we get $u^{n+1}>0$ along with (3.31). Furthermore, it also implies

$$\int_{\Omega_c}u^{n+1}J(\xi,t_{n+1})d\xi=\int_{\Omega_c}u^0J(\xi,t_0)d\xi.$$

It follows from (3.33) that

$$E_0(\bar{\phi}^{n+1})+r^{n+1}=\big(E_0(\bar{\phi}^n)+r^n\big)\left(1+\frac{\delta tE_{diss}(\bar{u}^{n+1},\bar{\phi}^{n+1},\bar{\phi}^n,\dot{x})}{E[\bar{u}^{n+1},\bar{\phi}^{n+1}]+C_0}\right)^{-1}\ge 0. \tag{3.42}$$

Therefore, we derive from (3.34) and $E[\bar{u}^{n+1},\bar{\phi}^{n+1}]+C_0>0$ that $\eta^{n+1}\ge 0$, which, together with (3.33), implies the energy dissipation (3.40).

Now we denote $M:=\bar{E}^0$, then energy dissipation implies $\bar{E}^n\le M,\forall n$. Then, it follows from (3.34) and $E_1(u,\phi)+C_0\ge 1$ that

$$|\eta^{n+1}|=\frac{\bar{E}^{n+1}}{E[\bar{u}^{n+1},\bar{\phi}^{n+1}]+C_0}\le\frac{M}{E_0(\bar{\phi}^{n+1})+1}. \tag{3.43}$$

Therefore, by the fact that $\sqrt{A}\le A+1$ for all $A\ge 0$, we obtain

$$\sqrt{E_0(\phi^{n+1})}=|\eta^{n+1}|\sqrt{E_0(\bar{\phi}^{n+1})}\le M. \tag{3.44}$$

The proof is complete. □

4 Numerical experiments

In this section, we present numerical examples to validate our numerical schemes. We analyze the performance of our Fourier spectral moving mesh positivity preserving SAV (MMPPSAV) method for solving the Keller-Segel chemotaxis model with periodic boundary conditions in two spatial dimensions. For all examples, the spatial domain (x,y) is chosen as $[0,2\pi)\times[0,2\pi)$. The spatial domain is discretized by the Fourier spectral method, and the time step is chosen as $\delta t=10^{-4}$ unless stated otherwise. If not specified, we fix the diffusion constant $D=\gamma=\mu=1$, the chemotactic sensitivity $\chi=1$, and $\alpha=0.1$.

4.1 Numerical results for a parabolic-elliptic Keller-Segel model

In this subsection, we conduct numerical experiments for the parabolic-elliptic case ($\tau = 0$) using our MMPPSAV method. Here, we show two numerical examples with different initial masses and carry out two different mesh moving strategies.

In the first example, the initial condition is

$$u(x,y,0) = 4\exp\left(-\frac{(x-L/2)^2+(y-L/2)^2}{4}\right). \tag{4.1}$$

Note that in this classical Keller-Segel equations with initial condition (4.1), the solution blows up in finite time. We compute this system up to the point where the computation breaks down and take that time as the estimated blow-up time. In addition, we also wish to see that our algorithm preserves the energy dissipation properties during evolution. To ensure $r(t) > 1$ throughout the computation, we set $C_0 = 10^4$. Here, we choose the monitor function as

$$\omega = \left(1+5|\nabla_{\tilde{\xi}} u|^2\right)^{\frac{1}{2}}, \tag{4.2}$$

and the generic constant $\mu = 1$. Since in this situation, the initial solution is not strongly peaked, we do not implement the MMPDEs to get an initial mesh before starting the numerical simulation. Instead, we implement one step of MMPDE to update the mesh at every time step and set the MMPDE time step equal to the physical time step, $\Delta t = \delta t = 10^{-4}$.

Fig. 1 shows the solutions at $t = 1.2$, $t = 1.3$ (before blow up), $t = 1.4$ (near blow up), and $t = 1.445$ (the estimated blow up time), while Fig. 2 shows the corresponding mesh-point distributions. The estimated blow-up time $t \approx 1.445$ is close to the blow-up time $t \approx 1.491$ computed by the original positivity preserving SAV algorithm on a uniform 256×256 mesh. We can observe that before blow up ($t = 1.2, 1.3$), the solution is not yet strongly peaked, so although mesh points concentrate where gradients are large, they do not yet focus at the exact point of maximum density. When the solution is near blow-up time ($t = 1.4$) and the estimated blow-up time ($t = 1.445$), the mesh points increasingly concentrate near the blow-up point, illustrating the advantage of the moving mesh method for resolving blow-up behavior. Fig. 3 plots the evolution of $u_{\max}$ and the modified energy $\bar{E}^n$, demonstrating that the algorithm preserves the energy dissipation property well (mass conservation and positivity preserving can be seen easily in the procedure of this algorithm).

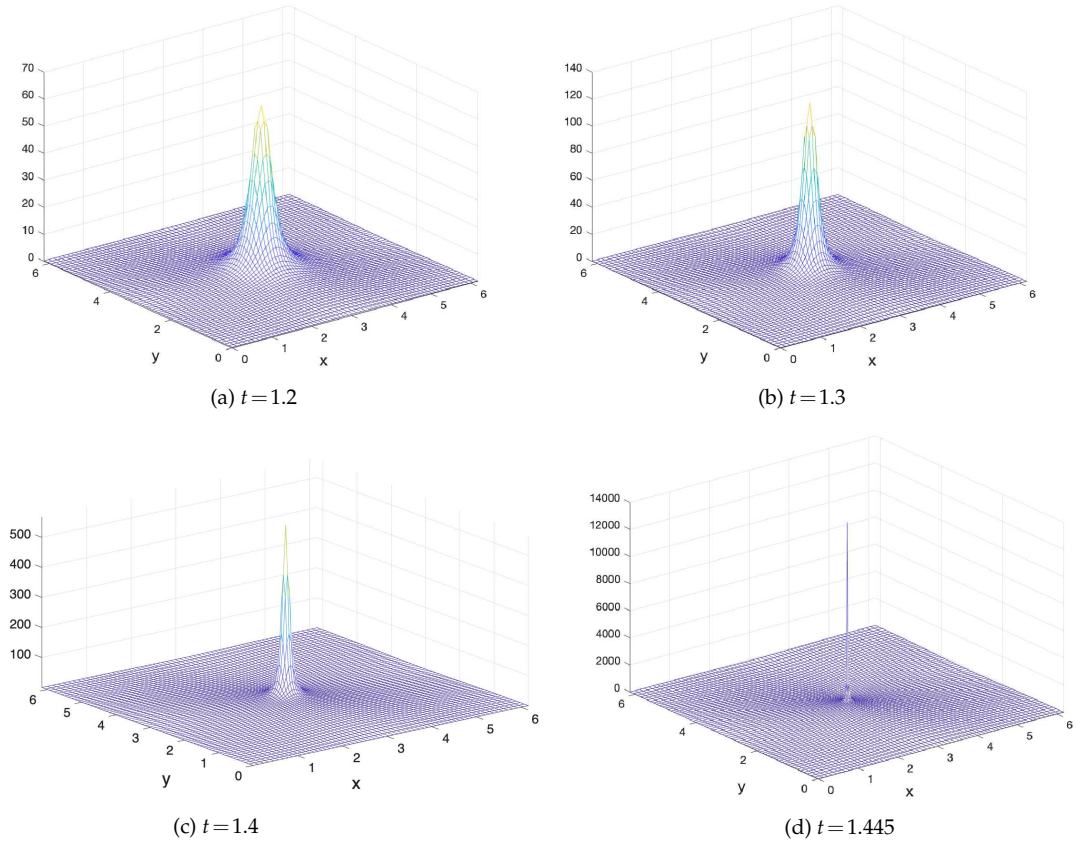

(a) $t=1.2$ (b) $t=1.3$

(c) $t=1.4$ (d) $t=1.445$

Figure 1: Solution evolution at different times.

In the second example, since the blow-up time could weigh heavily on the initial conditions, we consider a spiky initial condition

$$u(x,y,0)=500\exp(-30((x-L/2)^2+(y-L/2)^2)). \tag{4.3}$$

In this example, we choose $\delta t=10^{-5}$ and implement a different mesh moving strategy: first implement the MMPDE 100 times with a large artificial time step $\Delta t=10^{-2}$ to obtain an initial mesh-point distribution and then carry out the numerical simulation with $\Delta t=\delta t=10^{-5}$ and the same other settings in the first example. Fig. 4 shows the initial condition and the solution at the estimated blow up time $t\approx 4.7\times 10^{-3}$, which is very close to the time $t\approx 4.6\times 10^{-3}$ obtained by the original algorithm with 256×256 mesh. Fig. 5 shows the initial and final mesh-point distributions, while Fig. 6 shows the evolution of $u_{\max}$ and the modified energy.

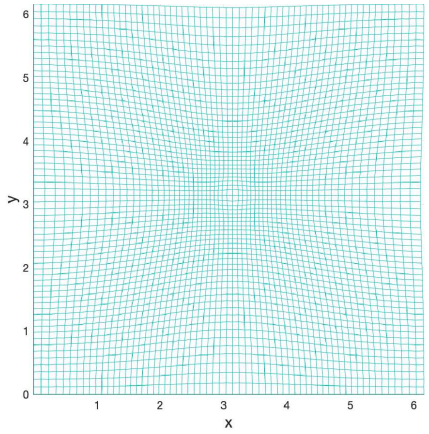

(a) $t=1.2$

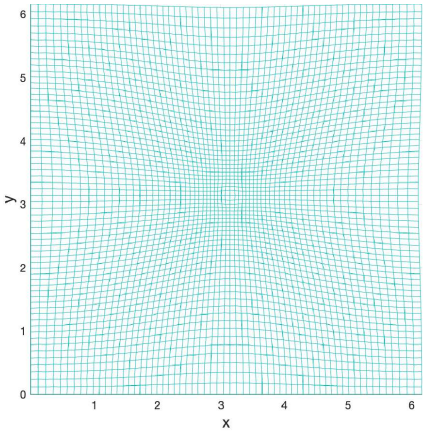

(b) $t=1.3$

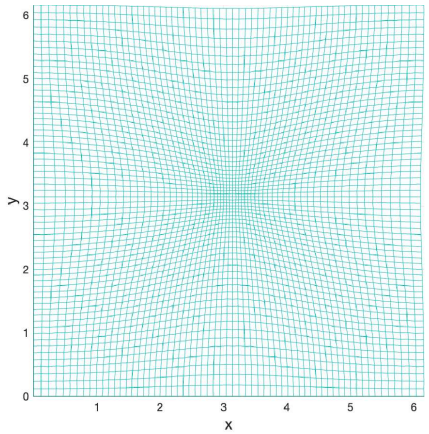

(c) $t=1.4$

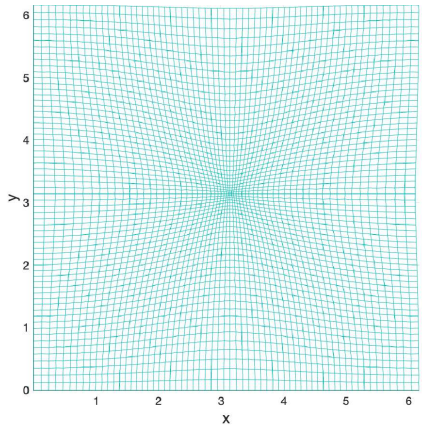

(d) $t=1.445$

Figure 2: Mesh-point distributions at different time corresponding to Fig. 1.

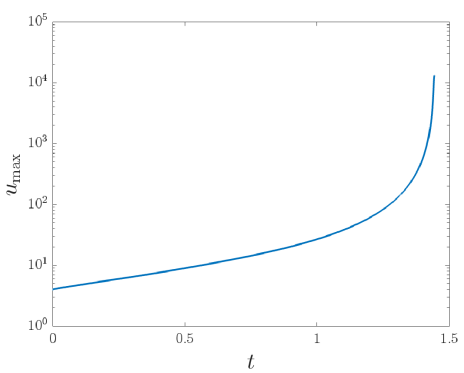

(a) $u_{\max}$

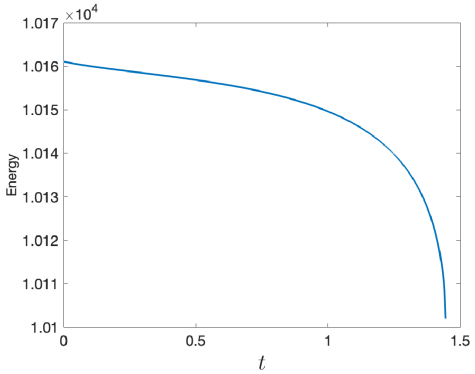

(b) Modified energy

Figure 3: The evolution of $u_{\max}$ and modified energy.

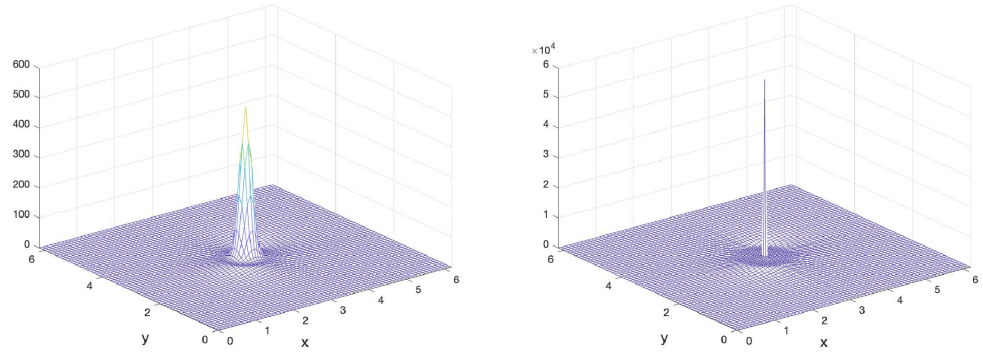

(a) $t=0$ (b) $t=4.7e^{-3}$

Figure 4: Initial solution and solution at the estimated blow-up time.

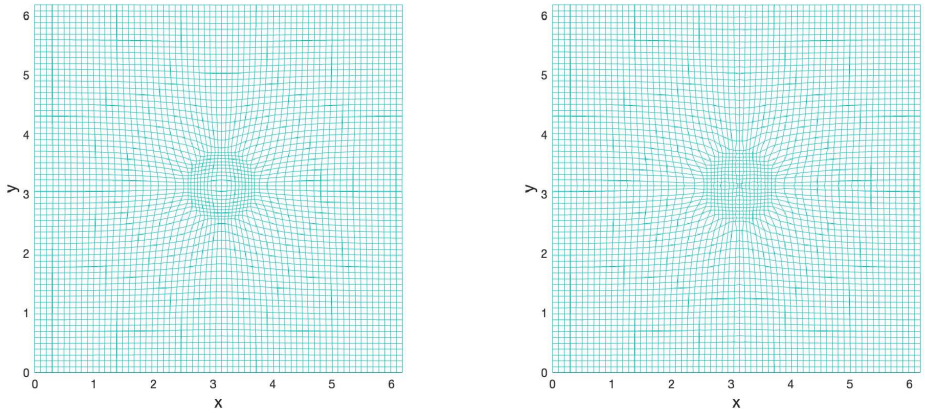

(a) $t=0$ (b) $t=4.7e^{-3}$

Figure 5: Mesh-point distribution at initial and final time corresponding to Fig. 4.

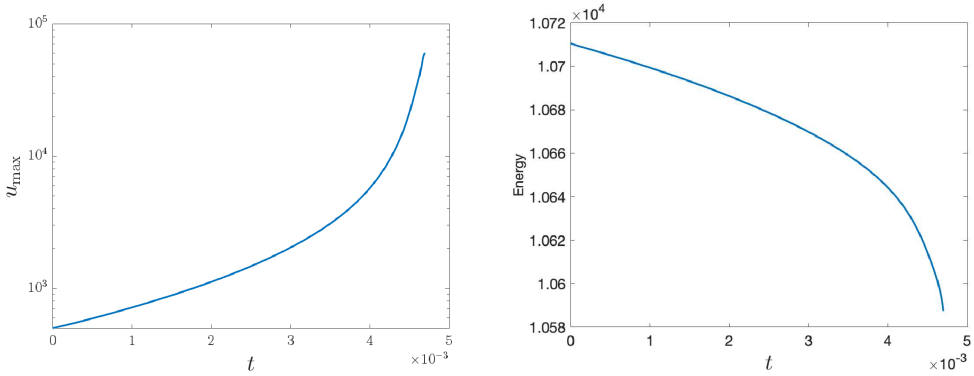

(a) $u_{\max}$ (b) Modified energy

Figure 6: The evolution of $u_{\max}$ and modified energy.

4.2 Numerical results for a parabolic-parabolic Keller-Segel model

Next, we test the parabolic-parabolic ($\tau > 0$) system. We set $\tau = 1$ and take the initial condition

$$u(x,y,0) = \phi(x,y,0) = 4\exp\left(-\frac{(x-L/2)^2+(y-L/2)^2}{4}\right). \tag{4.4}$$

The time step is $\delta t = 10^{-4}$ and we implement one step MMPDE to update the mesh per time step with $\Delta t = \delta t$. The monitor function is the same as in (4.2), and we choose the generic constant $\mu = 0.1$ for the MMPDE. Fig. 7 shows the solution

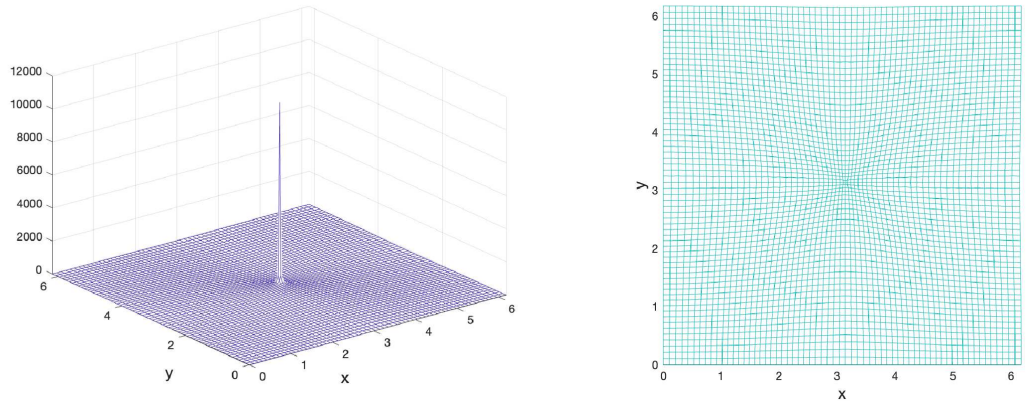

(a) Solution (b) Mesh

Figure 7: Solution and mesh distribution at the estimated blow up time $t = 2.034$.

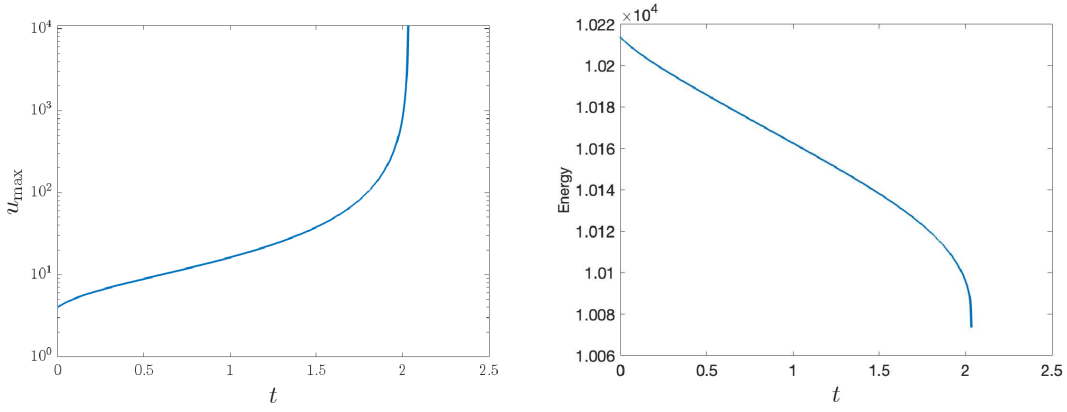

(a) $u_{\max}$ (b) Modified energy

Figure 8: The evolution of $u_{\max}$ and modified energy.

and mesh-point distribution at the estimated blow-up time $t \approx 2.034$. We observe that under the smaller generic constant μ, the mesh concentrates less densely than in the first example (see Fig. 2 (d)). Fig. 8 displays the evolution of $u_{\max}$ and the modified energy.

5 Conclusion

We have proposed and tested a numerical framework that couples a linear positivity preserving SAV scheme with Fourier spectral spatial discretization and a MMPDE-based moving mesh method to address the two principal numerical challenges posed by the Keller-Segel system: preserving the model's structural invariants and resolving highly localized, near-singular solution features. The Fourier implementation of MMPDE should change a little in computing the gradient in the monitor function for this blow-up case. We demonstrate that the moving mesh positivity preserving SAV scheme preserves mass and inherits the positivity preserving and energy dissipation features of the original scheme, provided the moving mesh remains non-overlapping. These properties are important for physical fidelity and numerical stability when simulating chemotactic aggregation. Numerical experiments verify that the proposed method captures sharp spike profiles and provides more reliable estimates of blow-up behavior than comparable fixed-mesh approaches. Additional work can be done by extending it to higher-order schemes and higher dimensions.

Acknowledgments

The computations were performed using the HKU ITS research computing facilities. We would like to thank Professor Qiang Du for stimulating discussions.

Z. Zhang was partly supported by the Hong Kong RGC Grant (Project No. 17300325), and by the Seed Funding Programme for Basic Research (HKU).

References

[1] L. Almeida, F. Bubba, B. Perthame, and C. Pouchol, *Energy and implicit discretization of the Fokker-Planck and Keller-Segel type equations*, Netw. Heterog. Media 14 (2019), 23–41.

[2] C. J. Budd, R. Carretero-González, and R. D. Russell, *Precise computations of chemotactic collapse using moving mesh methods*, J. Comput. Phys. 202 (2005), 463–487.

[3] V. Calvez and L. Corrias, *The parabolic-parabolic Keller-Segel model in* $\mathbb{R}^2$, Commun. Math. Sci. 6 (2008), 417–447.
[4] J. A. Carrillo, A. Chertock, and Y. Huang, *A finite-volume method for nonlinear nonlocal equations with a gradient flow structure*, Commun. Comput. Phys. 17 (2015), 233–258.
[5] W. Chen, Q. Liu, and J. Shen, *Error estimates and blow-up analysis of a finite-element approximation for the parabolic-elliptic Keller-Segel system*, Int. J. Numer. Anal. Model. 19 (2022), 275–298.
[6] A. Chertock and A. Kurganov, *A second-order positivity preserving central-upwind scheme for chemotaxis and haptotaxis models*, Numer. Math. 111 (2008), 169–205.
[7] Y. Di, R. Li, T. Tang, and P. Zhang, *Moving mesh finite element methods for the incompressible Navier-Stokes equations*, SIAM J. Sci. Comput. 26 (2005), 1036–1056.
[8] Y. Di and P. W. Zhang, *Moving mesh kinetic simulation for sheared rodlike polymers with high potential intensities*, Commun. Comput. Phys. 1 (2006), 859–873.
[9] Y. Epshteyn, *Upwind-difference potentials method for Patlak-Keller-Segel chemotaxis model*, J. Sci. Comput. 53 (2012), 689–713.
[10] F. Filbet, *A finite volume scheme for the Patlak-Keller-Segel chemotaxis model*, Numer. Math. 104 (2006), 457–488.
[11] W. M. Feng, P. Yu, S. Y. Hu, Z. K. Liu, Q. Du, and L. Q. Chen, *Spectral implementation of an adaptive moving mesh method for phase-field equations*, J. Comput. Phys. 220 (2006), 498–510.
[12] W. M. Feng, P. Yu, S. Y. Hu, Z. K. Liu, Q. Du, and L. Q. Chen, *A Fourier spectral moving mesh method for the Cahn-Hilliard equation with elasticity*, Commun. Comput. Phys. 5 (2009), 582–599.
[13] Y. Giga, N. Mizoguchi, and T. Senba, *Asymptotic behavior of type I blowup solutions to a parabolic-elliptic system of drift-diffusion type*, Arch. Ration. Mech. Anal. 201 (2011), 549–573.
[14] M. A. Herrero and J. J. L. Velázquez, *A blow-up mechanism for a chemotaxis model*, Ann. Sc. norm. super. Pisa - Cl. sci. 24 (1997), 633–683.
[15] F. Huang and J. Shen, *Bound/Positivity preserving and energy stable scalar auxiliary variable schemes for dissipative systems: Applications to Keller-Segel and Poisson-Nernst-Planck equations*, SIAM J. Sci. Comput. 43 (2021), A1832–A1857.
[16] W. Huang, *Practical aspects of formulation and solution of moving mesh partial differential equations*, J. Comput. Phys. 171 (2001), 753–775.
[17] W. Huang and R. D. Russell, *Analysis of moving mesh partial differential equations with spatial smoothing*, SIAM J. Numer. Anal. 34 (1997), 1106–1126.
[18] W. Huang and W. Sun, *Variational mesh adaptation II: Error estimates and monitor functions*, J. Comput. Phys. 184 (2003), 619–648.
[19] E. F. Keller and L. A. Segel, *Initiation of slime mold aggregation viewed as an instability*, J. Theor. Biol. 26 (1970), 399–415.
[20] E. F. Keller and L. A. Segel, *Model for chemotaxis*, J. Theor. Biol. 30 (1971), 225–234.

[21] E. F. Keller and L. A. Segel, *Traveling bands of chemotactic bacteria: A theoretical analysis*, J. Theor. Biol. 30 (1971), 235–248.

[22] P. G. Lemarié-Rieusset, *Small data in an optimal Banach space for the parabolic-parabolic and parabolic-elliptic Keller-Segel equations in the whole space*, Adv. Differential Equations 18(11/12) (2013), 1189–1208.

[23] R. Li, T. Tang, and P. Zhang, *Moving mesh methods in multiple dimensions based on harmonic maps*, J. Comput. Phys. 170 (2001), 562–588.

[24] R. Li, T. Tang, and P. Zhang, *A moving mesh finite element algorithm for singular problems in two and three space dimensions*, J. Comput. Phys. 177 (2002), 365–393.

[25] X. H. Li, C.-W. Shu, and Y. Yang, *Local discontinuous Galerkin method for the Keller-Segel chemotaxis model*, J. Sci. Comput. 73 (2017), 943–967.

[26] J. A. Mackenzie and M. L. Robertson, *A moving mesh method for the solution of the one-dimensional phase-field equations*, J. Comput. Phys. 181 (2002), 526–544.

[27] N. Mizoguchi, *Global existence for the Cauchy problem of the parabolic-parabolic Keller-Segel system on the plane*, Calc. Var. Partial Differ. Equ. 48 (2013), 491–505.

[28] B. Perthame, *Transport Equations in Biology*, Springer Science & Business Media, 2006.

[29] J. Shen and J. Xu, *Unconditionally bound preserving and energy dissipative schemes for a class of Keller-Segel equations*, SIAM J. Numer. Anal. 58 (2020), 1674–1695.

[30] P. Souplet and M. Winkler, *Blow-up profiles for the parabolic-elliptic Keller-Segel system in dimensions $n \geq 3$*, Commun. Math. Phys. 367 (2019), 665–681.

[31] M. Sulman and T. Ngyuen, *A positivity preserving moving mesh finite element method for the Keller-Segel chemotaxis model*, J. Sci. Comput. 80 (2019), 649–666.

[32] T. Takeuchi, *The Keller-Segel system of parabolic-parabolic type in homogeneous Besov spaces framework*, J. Differ. Equ. 298 (2021), 609–640.

[33] T. Tang, *Moving mesh methods for computational fluid dynamics*, Contemp. Math. 383 (2005), 141–173.

[34] G. Zhou and N. Saito, *Finite volume methods for a Keller-Segel system: Discrete energy, error estimates and numerical blow-up analysis*, Numer. Math. 135 (2017), 265–311.